HEFAT2014
10th International Conference on Heat Transfer, Fluid Mechanics and Thermodynamics
14 – 26 July 2014
Orlando, Florida

FEATURES OF FLOW AROUND THE LEADING EDGE OF A CIRCULAR CYLINDER

Qin Sun[1], Md. Mahbub Alam[1,2,]*, C.W. Wong[1] and Y. Zhou[1]

[1]Institute for Turbulence-Noise-Vibration Interaction and Control
Shenzhen Graduate School, Harbin Institute of Technology
Shenzhen 518055, China

[2]Key Lab of Advanced Manufacturing Technology
School of Mechanical Engineering and Automation
Shenzhen Graduate School, Harbin Institute of Technology
Shenzhen 518055, China
*Email: alamm28@yahoo.com; alam@hitsz.edu.cn

ABSTRACT

Axial flow over a circular cylinder is very complex, particularly around the leading edge of the cylinder, comprising separation bubble/cavitation, shear-layer reattachment, etc. Pressure fluctuations in the separation region may induce structural vibrations and generate noise. This paper presents the results of wall pressure measurement and flow visualization done around the cylinder leading edge with blunt, conical and hemispherical noses at Reynolds number (Re_D, based on cylinder diameter D) ranging from 1.5×10^3 to 4.2×10^4. The yaw angle α is varied from 0° (axial) to 3.5°. Attention has been paid to investigate the effects of nose shape, Re_D and α on the flow features as well as time-mean pressure coefficient C_p and fluctuating (rms) pressure coefficient C_p'. At α = 0°, blunt nose engenders longer reattachment length x_R, wider bubble width W and shorter transition length x_{Tr}, compared with conical and hemispherical noses. C_p and C_p' are found to be highly sensitive to Re_D for hemispherical nose. Blunt nose presents highest C_p', while hemispherical nose corresponds to the lowest C_p'. With increasing α from 0° to 3.5°, C_p declines and C_p' increases for both blunt and conical noses, while those for hemispherical nose vary less regularly. A slight increase in α influences the flow separation with enhanced x_R and W, and reduced x_{Tr} for all the three noses.

INTRODUCTION

The occurring of separation and reattachment of shear layer widely prevails both in nature and in many different engineering applications, such as aircraft fuselages, submarines, missiles, road vehicles, under-water vehicles and airfoils etc. When a shear layer separating from a point reattaches to another point on the same body, a separation bubble forms where pressure is highly negative. In many practical situations, the presence of the separation bubble has a significant influence on performances of devices or systems and results in vibration and noise.

A number of works on the features of the flow separation and reattachment region over a blunt cylinder in axial flow have been done in the literature (e.g. [1-5]), while a cylinder with an yaw angle α has attracted little attention. It has been confirmed that the most striking effect of α is the substantial asymmetry of the mean velocity field which may occur even at very small α [6, 7]. The considerable deviations from axisymmetry are also observed on the wall-pressure fluctuations [8]. Unfortunately, the previous researchers focused predominantly on the effects of small α on the fully developed turbulent region, away from the leading edge.

NOMENCLATURE

α	[°]	yaw angle
C_p	[-]	time-mean pressure coefficient
C_p'	[-]	fluctuating pressure coefficient
D	[mm]	cylinder diameter
E_p'	[W/Hz]	Fourier energy
f	[Hz]	Fourier frequency
x_{Tr}	[mm]	transition length, i.e. axial distance between separation and transition
Re_D	[-]	Reynolds number based on cylinder diameter
Re_θ	[-]	Reynolds number based on momentum thickness
U_∞	[m/s]	free stream velocity
W	[mm]	the width of the separation bubble
x	[mm]	axial distance from the stagnation point
x_R	[mm]	reattachment length

Wall pressure fluctuations in the separation region may generate considerable noise. Indeed, the pressure fluctuation in the reattachment region on an axisymmetric body is about ten times higher than that in the fully developed turbulent flow region [9]. While some studies on various flow configurations, i.e. flow over a flat plate with a blunt leading edge [10], flow over a normal flat plate with a long central splitter plate [11], flow over a backward-facing step [12], identified different characteristic frequencies of unsteadiness persisting in the separation region, some [13, 14] did not. Obviously, a disparity between the results exists.

Reynolds number effects have been performed on a flat plate, swept and unswept bumps with $Re_\theta = 1.4 \times 10^3 \sim 2.4 \times 10^4$ [15], outside of a wing/body junction with $Re_\theta = 5.94 \times 10^3$ and 2.32×10^4 [16], and on a smoothly contoured ramp with $Re_\theta = 1.1 \times 10^3 \sim 2.0 \times 10^4$ [17]. A general conclusion is made that the mean flow properties are weakly dependent on Reynolds number, whereas second order quantities are significantly dependent. Song and Eaton [17] studied Reynolds number effects on the features of separation over a smoothly contoured ramp. They found that the mean separation and reattachment positions change barely, except for very low Reynolds number ($Re_\theta \leq 3.0 \times 10^3$) at which the separated shear layer is not fully turbulent. An increase in Reynolds number, however, enhances Reynolds stress. It is noteworthy that studies on the effects of Reynolds number on a cylinder in axial flow or at a yaw angle are very limited.

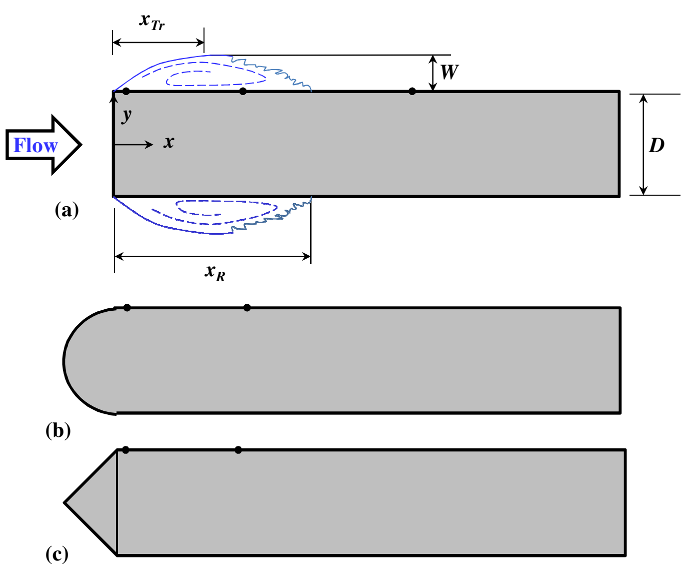

Figure 1 Sketches of models. (a) Blunt cylinder and definitions of reattachment length x_R, bubble width W and transition length x_{Tr},. (b) Hemispherical-nose cylinder. (c) Cone-nose cylinder. Small solid circles denote the pressure tap positions.

The forebody (nose) geometry has a considerable effect on the flow separation and reattachment. It could determine the separation points, such as blunt and conical noses separate the shear layer from their sharp edges, and hemispherical nose may do it not from a fixed point, but from different point depending on Reynolds number. Flow field near the leading edge of a blunt cylinder was examined at some particular Re_D in the literature (e.g., [1-5, 18]), while Re_D effects on the surface pressure fluctuation in the flow separation region is not yet well understood for not only blunt nose, but also cone and hemispherical noses. The cone nose model has been extensively studied as a model of projectiles or missiles at very high Reynolds numbers (i.e. subsonic, sonic and supersonic) and high angles of attack where the flow separation and vortex shedding induce a large unsolicited side force. The incident flow on the cylinder-like submarines in reality is always not axial, but may be at a small α. The effect of α on the leading edge flow behavior is, however, not well documented. In fact, the pressure fluctuation at a point is the integrated effect of the velocity fluctuation, hence giving an overall picture of the flow around the point. This paper focused on the effects of nose shape as well as α on the flow features around the leading edge in order to improve our understanding of the flow separation and reattachment mechanisms on such configurations.

The objective of this paper is to examine the surface pressure fluctuation and the behavior of the flow around the leading edge of a circular cylinder with blunt, conical, hemispherical noses, with Re_D ranging from 1.5×10^3 to 4.2×10^4. Apart from a cylinder in axial flow, the cylinder with α = 2.0° and 3.5° are also studied. Time-mean and rms pressures are measured at points immediately behind the shear-layer separation, ahead of the reattachment and following the reattachment (Figure 1a) and Re_D effects are discussed. Furthermore, flow visualization experiment is also conducted to extract the behaviors of shear layer and separation bubble.

EXPERIMENTAL DETAILS

Experiments were performed in a closed-circuit wind tunnel with the test section of 5.5 m in length, 0.8 m in width and 1.0 m in height. The flow non-uniformity was within ± 0.1% (rms) within the central cross sectional area of 0.75 m × 0.95 m in the test section, and the longitudinal turbulence intensity was less than 0.2% in the absence of the cylinder. The free-stream velocity, U_∞, was varied from 3.0 to 46.8 m/s.

Four models were used in the present experiments. Three of them had the same diameter of D = 16 mm, with blunt, conical, and hemispherical nose, respectively. Another of D = 7.5 mm with blunt nose was adopted so that investigated Re_D could be reduced to 3.3×10^3.

The cylinder positioned horizontally at the centerline of the test section was a cantilever supported by means of a vertical stainless steel strut attached to a rotating plate with degree scale, so that any α can be achieved. To avoid the model vibration induced by the wind tunnel wall, the rotating plate was set onto a metal trestle which was across the test section without touching the wind tunnel wall. By the rotating the plate, the investigated α of 0°, 2.0° and 3.5° could be adjusted to.

It is known that x_R/D is larger than 1.5 at least over a wide range of Re_D for a blunt cylinder in axial flow [1-5, 18]. We are interested to know the difference in pressure fluctuations (i) immediately behind the separation, (ii) around the center of the separation bubble, and (iii) behind the reattachment. Therefore, three pressure taps on the cylinder of D = 7.5 mm at x/D = 0.15, 1.0 and 2.5, respectively, were made (Figure 1). The cylinders of D = 16 mm were, however, furnished with two pressure taps only at x/D = 0.15 and 1.0, respectively. Therefore, data for x/D = 2.5 will be available at $Re_D < 2.5 \times 10^4$ only. All the pressure taps were connected to a pressure transducer (Toyoda PD104K) through a small cavity between the pressure taps and the transducer diaphragm. The transducer had a high accuracy of ± 0.4% and an excellent frequency response up to 450 Hz. For yaw angle cases, the pressure taps were on the leeward side. The wall pressure data were acquired with a sampling frequency of 3 kHz by a National Instruments data acquisition board. The low-pass cutoff frequency was set at 1 kHz.

In order to further study the flow separation features, flow visualization on the leading edge was performed by means of a PIV system. To visualize the separated flow, the smoke particles were released into the flow field through a hole of 0.8 mm in diameter near the leading edge stagnation point. The particles were generated by a high volume liquid droplet seeding generator (Dantec Dynamics 10F03). The flow is illuminated in the leading edge area with a laser sheet from the side of the wind tunnel test section, and a high speed CCD camera was used to capture images of the targeted area.

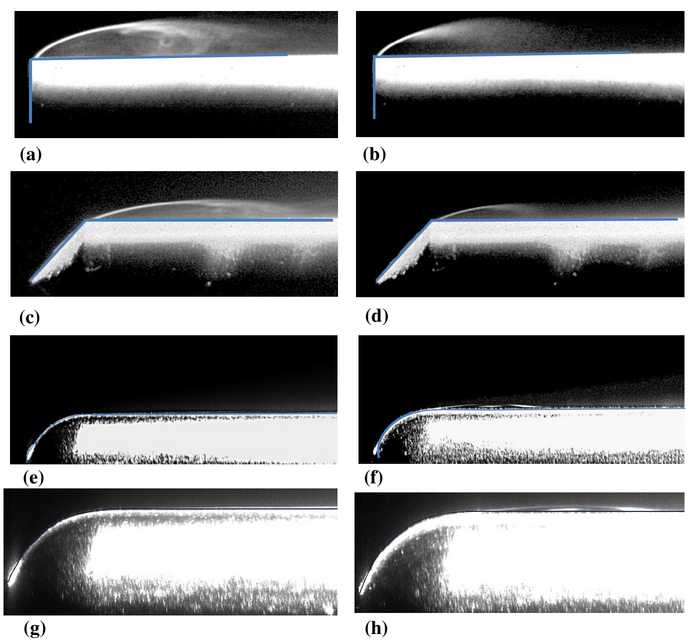

Figure 2 Flow visualization results for the three noses at α = 0°. (a, b) blunt, (c, d) conical, (e, f) hemispherical, at Re_D = (3.0×10^3, 1.0×10^4), respectively. (g, h) are the zoomed-in view of (e, f), respectively.

RESULTS AND DISCUSSION

Features of bubble

Figure 2 presents flow visualization results obtained for three nose shapes. Figures 2(a, b, c, d, e, f) are shown in the same scale, while Figures 2(g, h) are enlarged view of Figures 2(e, f), respectively. What is conspicuous in the figure is that reattachment length x_R (i.e., streamwise bubble size), shear layer transition length x_{Tr}, bubble width W (lateral bubble size) all shrinks for both blunt and conical noses, when Re_D is increased from 3.0×10^3 to 1.0×10^4. For hemispherical nose separation was not observed at $Re_D = 3.0 \times 10^3$, but it occurs at $Re_D = 1.0 \times 10^4$, followed by a reattachment.

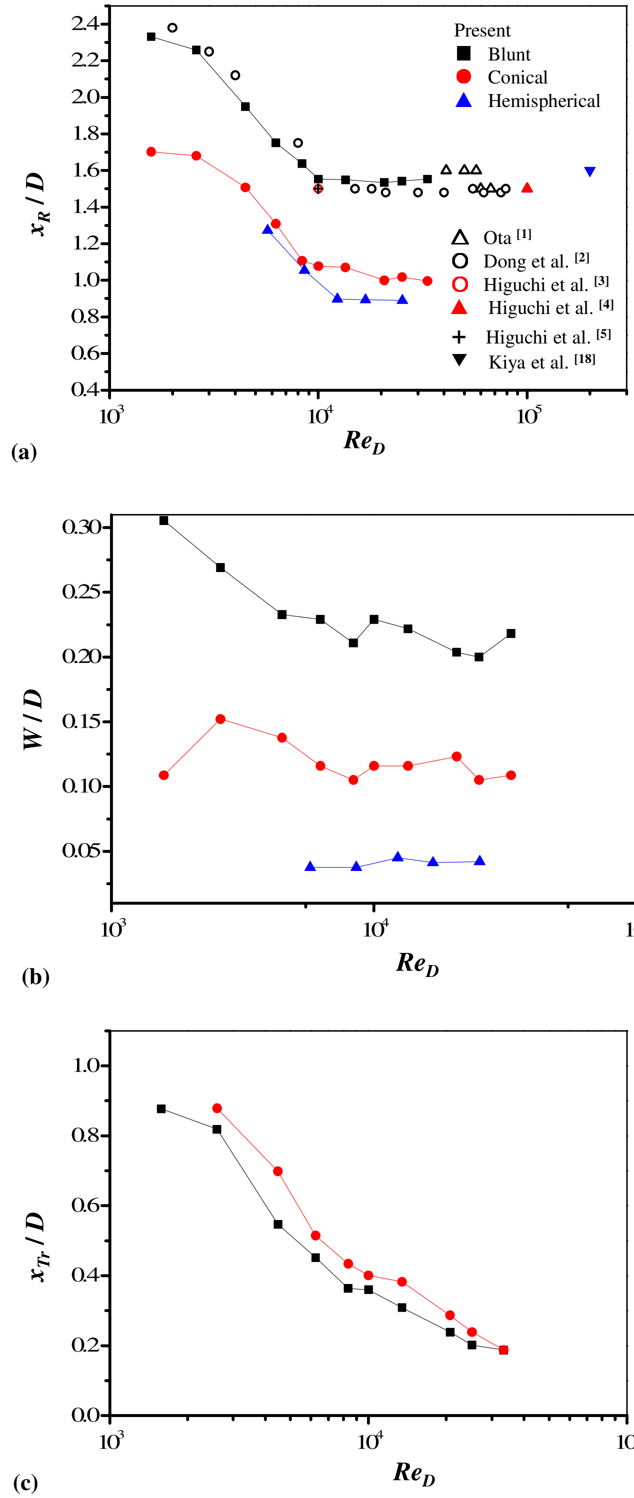

Figure 3 Effects of Re_D on (a) x_R/D, (b) W/D, (c) x_{Tr}/D, at $\alpha = 0°$.

Figure 3(a) displays the variation of x_R/D with Re_D at $\alpha = 0°$ for the three noses, incorporating blunt nose data available in the literature. Blunt nose x_R/D measured presently at $Re_D < 10^4$ is slightly lower than that measured by Dong et al.'s [2], which is attributed to the fact that the present free-stream turbulence intensity (0.2%) is higher than their's (0.08%). As we know, a larger free-stream turbulence intensity could significantly influence the transition in the shear layer, leading to shorter x_R/D in our measurements. On the other hand, x_R/D fluctuates between 1.5 and 1.6 at $Re_D > 10^4$, which accords well with previous measurements. The x_R/D for conical nose is smaller than that for blunt nose while larger than that for hemispherical nose, both having similar trends with blunt nose. The x_R/D value for conical nose at $Re_D > 10^4$ is about 1.05~1.1, while that for hemispherical nose is about 0.9 for $Re_D > 1.22 \times 10^4$. The W/D shown in Figure 3(b) wanes with Re_D for both blunt and cone noses, particularly for $Re_D < 10^4$. It is, however, less sensitive to Re_D for $Re_D > 10^4$. The W/D for conical nose is about half of that for blunt nose, except at the lowest Re_D. That for hemispherical nose is much smaller. At a given Re_D, the decrease in both x_R/D and W/D with change in the nose would be connected to the flow separation angle defined as the angle between the free-stream and direction of flow at the separation. The blunt nose being bluffest renders a large separation angle, hence a large bubble size ($x_R/D \times W/D$). The size decays for conical nose and hemispherical nose accordingly. The effect of the nose on x_{Tr}/D is nevertheless opposite, being the smallest for blunt nose (Figure 3c). The transition in the shear layer was not observed for hemispherical nose in the Re_D range examined at $\alpha = 0°$, hence no data are given for hemispherical nose in Figure 3(c). So it can be concluded that, compared with conical and hemispherical noses, blunt nose has longer x_R/D (Figure 3a), wider W/D (Figure 3b) and shorter x_{Tr}/D (Figure 3c).

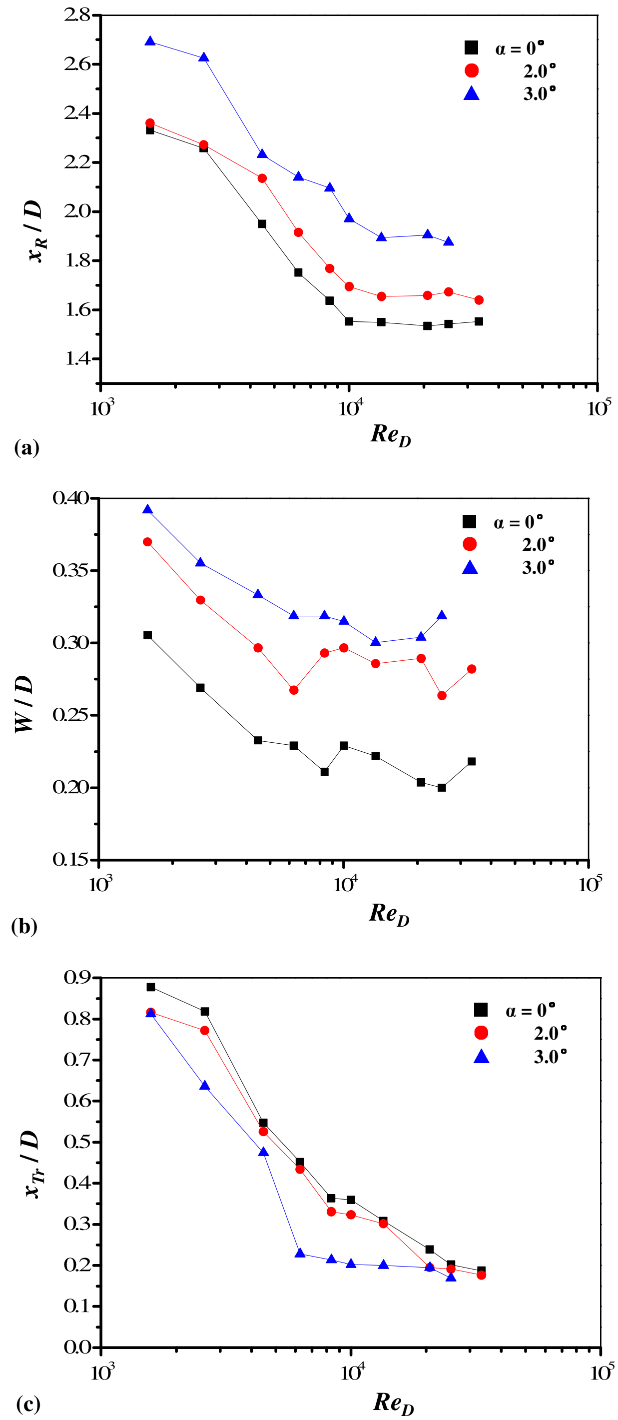

Yaw angle effect

Figure 4 compares x_R/D, W/D and x_{Tr}/D for $\alpha = 0°$, 2.0° and 3.5° for the three noses. Indeed, quantitative information on W/D and x_{Tr}/D was not found in the literature, hence not included. Although transition moves upstream with increase in α (Figure 4c, f, i) for the three nose shapes, W/D increases with α (Figure 4b, e, h) which results in an increase in x_R/D (Figure 4a, d, g). As the flow separates from the sharp edge for both blunt and conical noses, the variations of x_R/D, W/D and x_{Tr}/D show similarities in the two cases. The x_R/D, W/D and x_{Tr}/D all decline dramatically with Re_D for all tested α at $Re_D < 1.0 \times 10^4$ and they all attenuate for $Re_D > 1.0 \times 10^4$. On the other hand, for hemispherical nose the separation point is not fixed, but changes with Re_D and separation does not occur until $Re_D = 5.72 \times 10^3$.

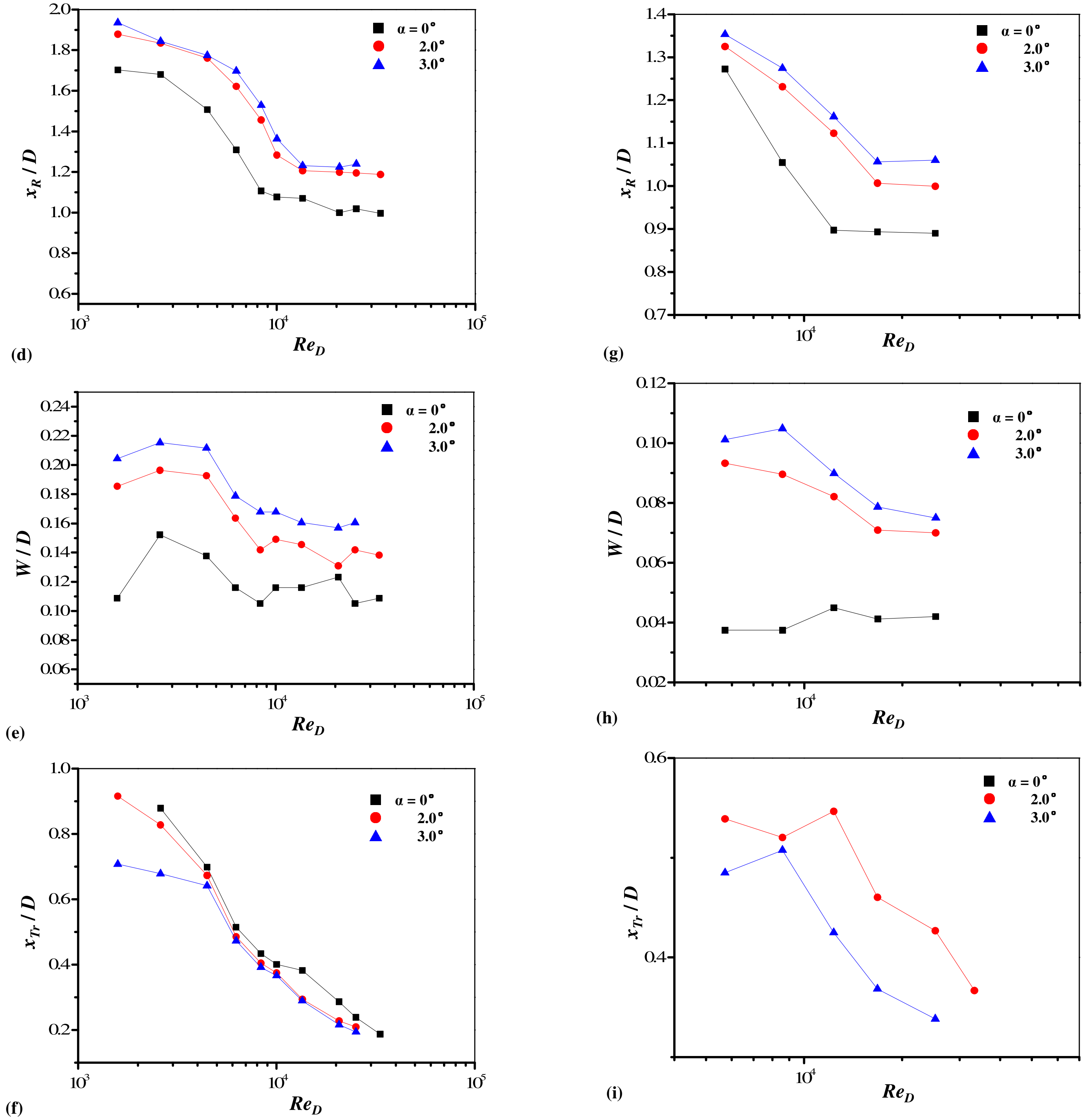

Figure 4 Effects of α on x_R/D, W/D and x_{Tr}/D, (a,b,c) blunt, (d,e,f) conical, (g, h, i) hemispherical.

Mean and fluctuating pressures

Figure 5 shows the effects of Re_D on time-mean surface-pressure coefficient C_p and fluctuating (rms) pressure coefficient C_p' at x/D = 0.15, 1.0 and 2.5 for blunt cylinder at α = 0°. It also includes data from the literature, showing validation of the present measurements. At $Re_D = 2.7 \times 10^3$ ~

1.0×10^4, C_p and C_p' at x/D = 1.0 decline and increase, respectively, which is attributed to the fact that the bubble size shrinks towards the leading edge with Re_D (as observed in the flow visualization) that enhances the intensity of the bubble. On the other hand, for $Re_D > 1.0 \times 10^4$, C_p and C_p' tend to be constant as a result of the bubble size being almost insensitive to Re_D. However, both C_p and C_p' at x/D = 0.15 augment slightly, because the shear layer near the separation narrows when Re_D is increased. While C_p at x/D = 0.15 and 1.0 ranges between -0.52 and -0.68, that at x/D = 2.5 is between -0.1 and 0.0. The observation implies that C_p magnitude is larger in the separation bubble than the downstream of the reattachment. With an increase in Re_D, C_p' at x/D = 2.5 wanes rapidly. The waning of C_p' results from the combined effect of shifts of both shear-layer transition and reattachment to the upstream.

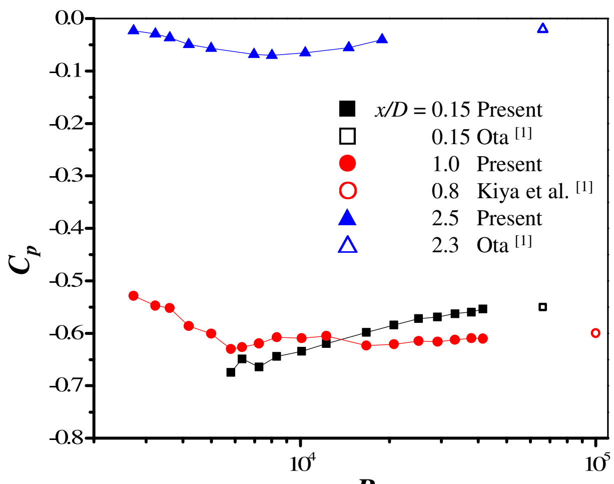

(a)

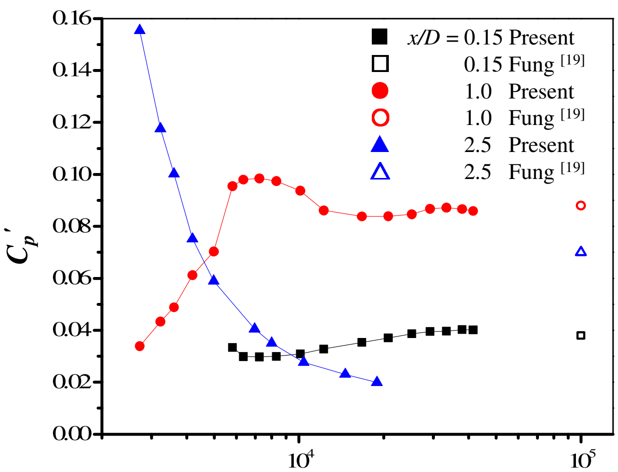

(b)

Figure 5 Dependences on Re_D of (a) C_p, and (b) C_p', at $\alpha = 0°$ for blunt nose.

Ota's [1] data measured at $x/D \approx 0.15$ and 2.3 ($Re_D = 6.62 \times 10^4$) and Kiya et al.'s [18] data at $x/D \approx 0.8$ ($Re_D = 10^5$), both accord well with our present measurements of C_p, following the C_p trends (Figure 5a). Meanwhile, the present results at x/D = 0.15 and 1.0 match Fung's [19] data measured at the same location ($Re_D = 10^5$) according to the trends of C_p', while the present C_p' at x/D = 2.5 shows a disparity compared with Fung's [19] data at x/D = 2.5 ($Re_D = 10^5$, see Figure 5b), which might be due to the fact that the boundary layer has been highly turbulent far downstream of the reattachment at high Re_D, leading to a higher level pressure fluctuation.

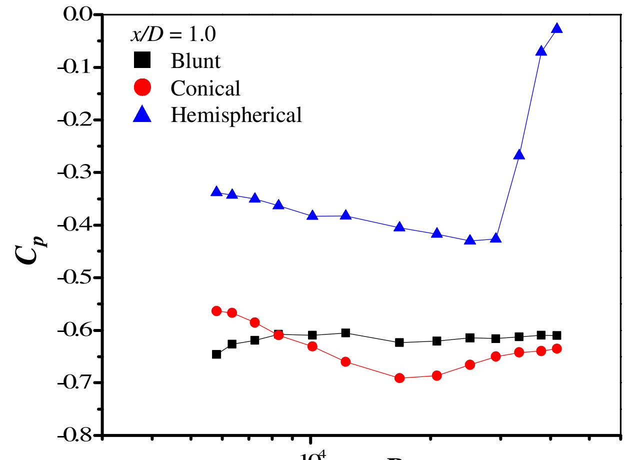

(a)

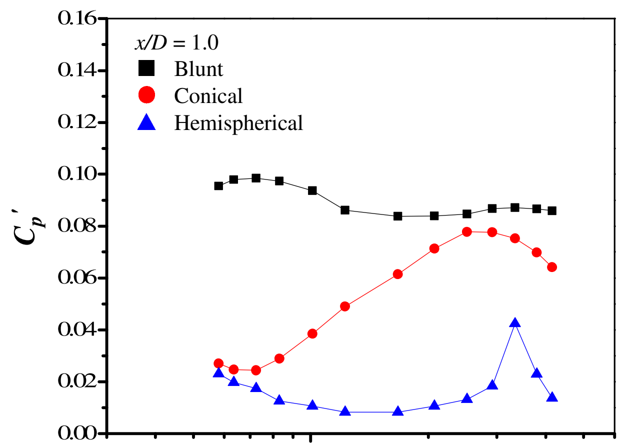

(b)

Figure 6 Dependences on Re_D for the three nose shapes (a) C_p and (b) C_p', at $\alpha = 0°$.

Figure 6 compares C_p and C_p' at x/D = 1.0 among the three noses. The magnitude of C_p is smaller for hemispherical nose and larger for conical nose except at $Re_D < 10^4$, compared to that for blunt nose. Furthermore, both C_p and C_p' are highly sensitive to Re_D for hemispherical nose, due to easy shift of the separation point with increasing Re_D. Blunt nose presents the highest C_p', while hemispherical nose corresponds to the lowest C_p'. For hemispherical nose, a sharp peak in C_p' variation at $Re_D = 3.3 \times 10^4$ is observed and C_p around the same Re_D recovers drastically. Both observations indicate that the reattachment occurs downstream and upstream of x/D = 1.0 for $Re_D < 3.3 \times 10^4$ and $Re_D > 3.3 \times 10^4$, respectively, and around x/D = 1.0 at $Re_D = 3.3 \times 10^4$. The flow visualization results indicate that $x_R/D \approx 0.90$ at $Re_D = 3.3 \times 10^4$ (see Figure 3a). Furthermore, it was observed that separation position occurs shortly downstream of x/D = 0. All the observations insinuate that the peak in C_p' Re_D = 3.3 × 10^4 is caused by the shear layer reattachment around x/D = 1.0. On the other hand, for blunt and conical noses, absences of recovery in C_p and sharp peak in C_p' suggest that the reattachment nestles beyond x/D = 1.0. An increase in C_p' with Re_D at x/D = 1.0 prevails for conical nose because the reattachment position proceeds and approaches x/D = 1.0, as can be seen in Figure 3(a).

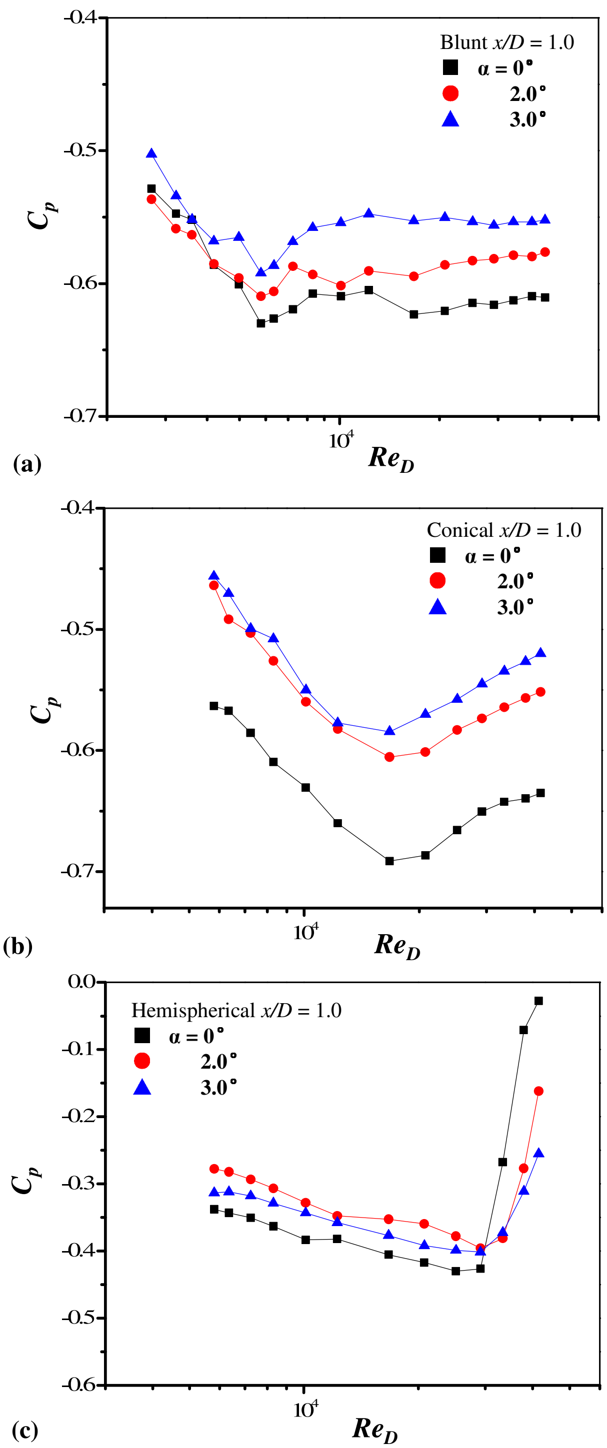

Figure 7 Effects of α on C_p for (a) blunt nose, (b) conical nose, and (c) hemispherical nose.

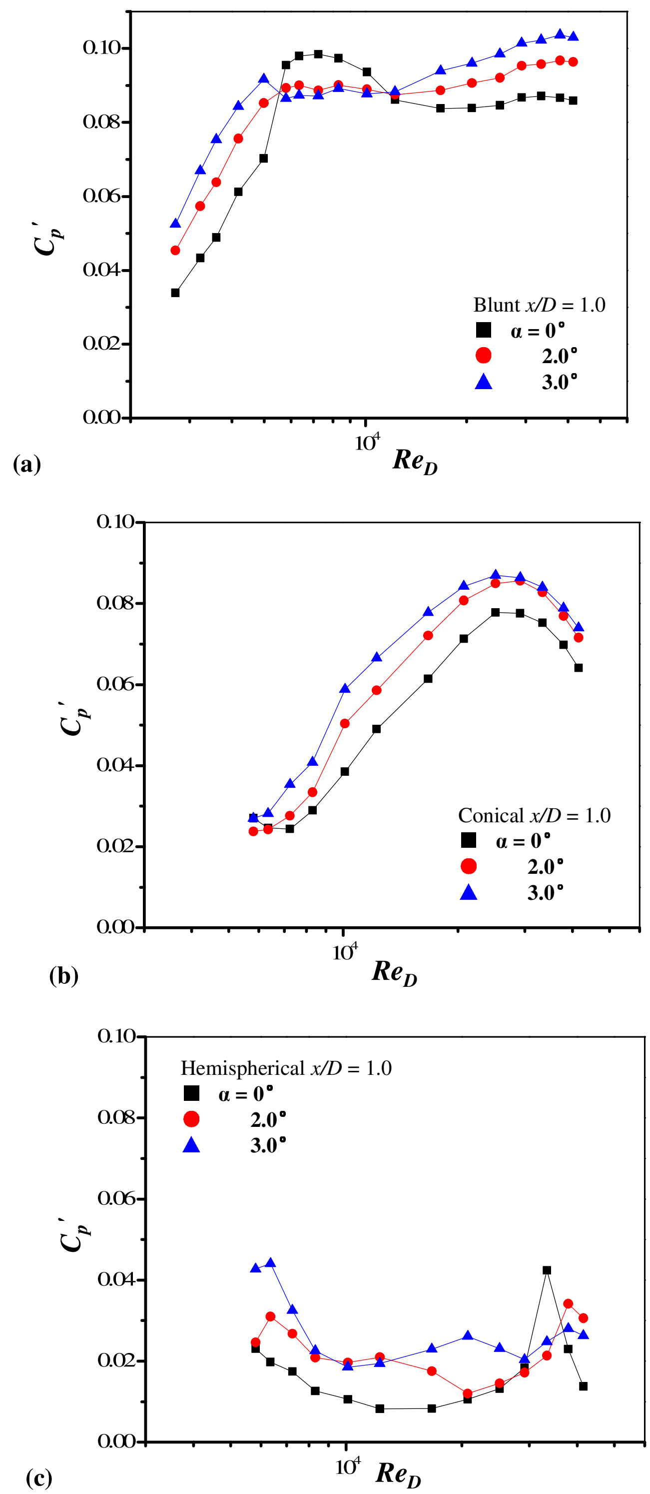

Figure 8 Effects of α on C_p' for (a) blunt nose, (b) conical nose, (c) hemispherical nose.

Figures 7 and 8 compare the effects of α on C_p and C_p', respectively, for the three noses. With increasing α from 0° to 3.5°, C_p magnitude reduces and C_p' is enhanced for both blunt and conical noses, while the magnitudes of C_p and C_p' for the hemispherical nose is small and the variation with α is irregular. Flow around the cylinder at $\alpha \neq 0°$ is highly three-dimensional and asymmetric around the cylinder axis, while that at $\alpha = 0°$ is symmetric. The normal component of the flow at $\alpha \neq 0°$ feeds flow in the bubble, resulting in C_p declining for both blunt and conical noses. With an increase in α, the bubble becomes larger due to enhanced x_R and W (see Figure 4a, b, d, e); hence C_p' augments accordingly. On the other hand, both separation and reattachment points change with α for hemispherical nose, leading to an irregular change in C_p and C_p'. Again C_p recovery and peak in C_p' are observed for $\alpha \neq 0°$ as well, but at higher Re_D. The observation again confirms that a greater α is accompanied by a longer x_R at a given Re_D.

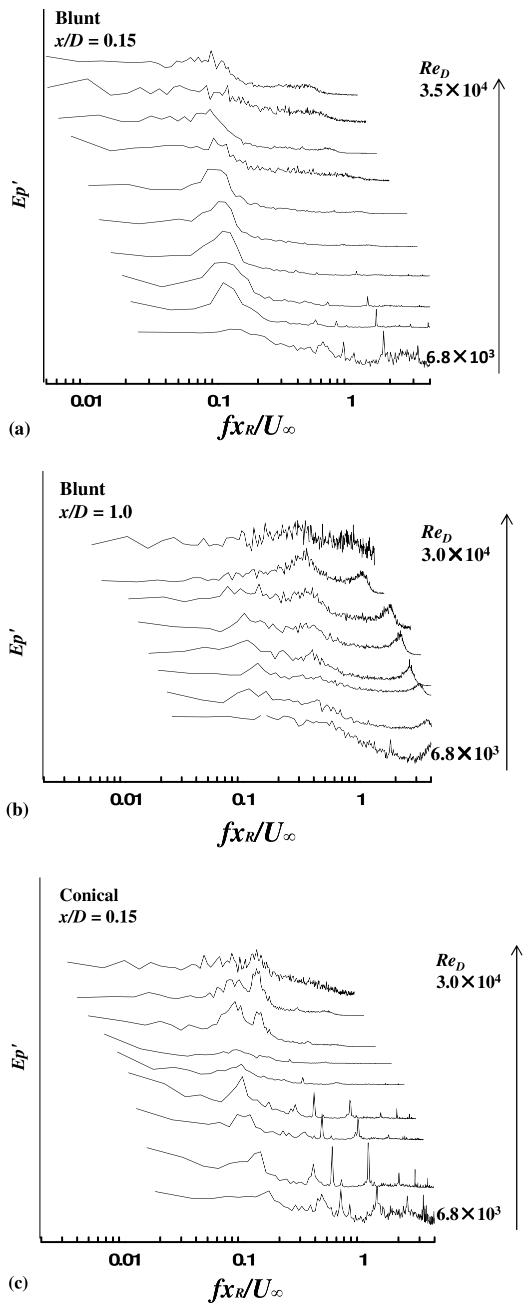

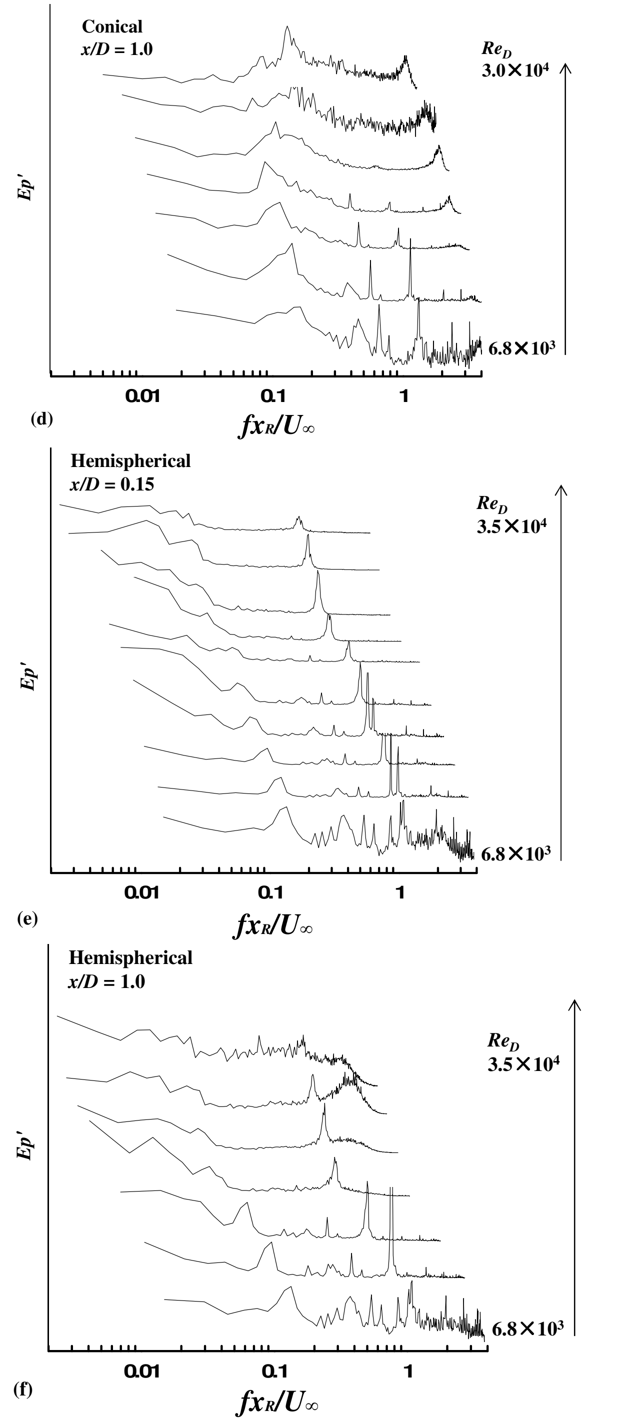

Figure 9 Power spectral density functions E_P' of fluctuating pressure for three nose shapes at $\alpha = 0°$**,** (a, c, e) $x/D = 0.15$ and (b, d, f) $x/D = 1.0$.

Flow unsteadiness

Figure 9 illustrates power spectral density functions E_P' of fluctuating pressure for the three noses at $x/D = 0.15$ and 1.0.

There are two frequencies that are noteworthy to be discussed. One is a low frequency, $fx_R/U_\infty \approx 0.1$ (Figure 9a) which appears shortly downstream of separation edge, and the other is a high frequency, $fx_R/U_\infty \approx 0.4$ (Figure 9b) which is detected in the reattachment region, both remain almost unchanged with Re_D. Kiya et al. [18] measured fluctuating pressure on a blunt leading edge of a circular cylinder in axial flow at $Re_D = 2.0 \times 10^5$, a low frequency of $fx_R/U_\infty \approx 0.1$ at $x/D = 0.18$ and a high frequency of $fx_R/U_\infty \approx 0.6$ at $x/D = 1.62$, which was at the reattachment, were detected. The low frequency is the same as the present, while the high frequency is higher than the present, which is because the high frequency increases gradually with increasing x/D in the reattachment region and the present pressure was measured upstream of reattachment at $x/D = 1.0$. The low frequency is associated with the flapping motion of the separated shear layer, while the high frequency is associated with the shedding of the large-scale eddies around the reattachment. The low frequency is however about $fx_R/U_\infty = 0.08 \sim 0.16$ and $0.03 \sim 0.13$ for conical and hemispherical noses, respectively, which decreases with Re_D for the latter case. The high frequency is not discernible for the conical and hemispherical noses, perhaps because they are much less bluff than the blunt one. Markedly high frequency peaks are observed in all the power spectra for the three nose shape cylinders, which is attributed to the fact that the frequency response of the pressure transducer is worse beyond 450 Hz.

CONCLUSIONS

Bubble features, C_p, C_p' and flow unsteadiness are examined for a cylinder with three different nose shapes, namely, blunt, cone and hemisphere in a wide range of $Re_D = 3.3 \times 10^3 \sim 5 \times 10^4$. While flow visualization is conducted to extract bubble features, C_p and C_p' measurements are performed at three different points on the cylinder, i.e., immediately behind the boundary layer separation, in the separation bubble and behind the shear layer reattachment.

Compared with conical nose and hemispherical nose, blunt nose has longer x_R/D, wider W/D and shorter x_{Tr}/D. C_p behind the reattachment is found to be smaller in magnitude compared to the other points measured. For the blunt cylinder, at $Re_D = 3.3 \times 10^3 \sim 10^4$, the change in bubble size plays a significant role in determining both C_p and C_p' in the separation bubble. Beyond Re_D of 10^4, C_p and C_p' in the separation bubble was less sensitive to Re_D because of the nearly unchanged bubble size. The magnitude of C_p is smaller for hemispherical nose and larger for conical nose compared to that for blunt nose. Furthermore C_p and C_p' are highly sensitive to Re_D for hemispherical nose, as a result of easy shift of the separation point with increasing Re_D. Blunt nose has highest C_p', while hemispherical nose has the lowest C_p'.

With increasing α from 0° to 3.5°, C_p declines and C_p' increases for both blunt and conical cases, while those for hemispherical nose vary less regularly. The most significant effect of α on flow is both x_R and W are enhanced, while x_{Tr} shrinks for all the three noses. The FFT analysis results of fluctuating pressure indicate that both low and high frequencies, normalized by x_R, appear for blunt nose, and remain almost unchanged with increasing Re_D. On the other hand, only the low frequency emerges for conical and hemisphere noses, decreasing with Re_D for the latter.

ACKNOWLEDGMENTS

Alam wishes to acknowledge supports given to him from the Research Grant Council of Shenzhen Government through grants JCYJ20120613145300404 and JCYJ20130402100505796.

REFERENCES

[1] Ota, T., An Axisymmetric Separated and Reattached Flow on a Longitudinal Blunt Circular Cylinder, *Journal of Applied Mechanics*, 1975, pp. 311-315.

[2] Dong, Y.F., Wei, Z.L., Xu, C., Jiang, X.Q., and Liao, Y.F., on Separated Shear Layer of Blunt Circular Cylinder, *Acta Mechanica Sinica*. Vol. 13, 1997, pp. 313-322.

[3] Higuchi, H., Sawada, H., van Langen, and Pieter, Flow over a Magnetically Suspended Cylinder in an Axial Free Stream, *AIAA Paper* 05-1078, 2005.

[4] Higuchi, H., van Langen, Sawada, H., and Tinney, C.E., Axial Flow over a Blunt Circular Cylinder with and without Shear Layer Reattachment, *Journal of Fluids and Structures*, Vol. 22, 2006, pp. 949-959.

[5] Higuchi, H., Sawada, H., and Kato, H., Sting-Free Measurements on a Magnetically Supported right Circular Cylinder aligned with the Free Stream, *Journal of Fluid Mechanics*, Vol. 596, 2008, pp. 49-72.

[6] Bücker, D., and Lueptow, R.M., The boundary layer on a slightly yawed cylinder, *Experiments in Fluids*, Vol. 25, 1998, pp. 487-490.

[7] Heenan, A.F., and Morrison, J.F., Turbulent boundary layers on axially inclined cylinders. Part 1. Surface-pressure/velocity correlations, *Experiments in Fluids,* Vol. 32, 2002, pp. 547-557.

[8] Snarski, S.R., Flow over yawed circular cylinders: Wall pressure spectra and flow regimes, *Physics of Fluids*, Vol. 16, 2004, pp. 344-359.

[9] Arakeri, V.H., A note on the transition observations on an axisymmetric body and some related fluctuating wall pressure measurement, *Journal of Fluids Engineering*, Vol. 97, 1975, pp. 82-87.

[10] Kiya, M., and Sasaki, K., Structure of a turbulent separation bubble, *Journal of Fluid Mechanics*, Vol. 137, 1983, pp. 83-113.

[11] Cherry, N.J., Hillier, R., and Latour, M.E.M.P., The unsteady structure of two-dimensional separated and reattaching flows, *Journal of Wind Engineering & Industrial Aerodynamics*, Vol. 11, 1983, pp. 95-105.

[12] Lee, I., and Sung, H.J., Characteristics of wall pressure fluctuations in separated and reattaching flow over a backward-facing step, *Experiments in Fluids*, Vol. 30, 2001, pp. 62-272.

[13] Ruderich, E., and Fernholz, H.H., An experimental investigation of a turbulent shear flow with separation, reverse flow and reattachment, *Journal of Fluid Mechanics*, Vol. 163, 1986, pp. 283-322.

[14] Yang, Z., and Abdalla, I.E., Effects of free-stream turbulence on a transitional separated-reattached flow over a flat plate with a sharp leading edge, *International Journal of Heat and Fluid flow*, Vol. 30, 2009, pp. 1026-1035.

[15] DeGraaff, D.B., and Eaton. J.K., Reynolds Number Scaling of the Turbulent Boundary Layer on a Flat Plate and on Swept and Unswept Bumps, *Report No. TSD-118, Stanford University, Stanford, Calif.*, January 1999.

[16] Olcmen, M.S., Simpson, R.L., and George, J., Some Reynolds number effects on two- and three-dimensional turbulent boundary layers, *Experiments in Fluids.* Vol. 31, 2001, pp. 219-228.

[17] Song, S., and Eaton, J.K., Reynolds number effects on a turbulent boundary layer with separation, reattachment, and recovery, *Experiments in Fluids*. Vol. 36, 2004, pp. 246-258.

[18] Kiya, M., Mochizuki, O., Tamura, H., Nozawa, T., Ishikawa, R., and Kushioka, K., Turbulence Properties of an Axisymmetric Separation-and-Reattaching Flow, *AIAA Journal*, Vol. 29, 1991, pp. 936-941.

[19] Fung, K.S., Unsteady Measurements near Leading Edge of Separated Flow, *JSME International Journal*, Vol. 39, 1996, pp. 354-360.